Chemical Physics 427 (2013) 106–110

Contents lists available at ScienceDirect

Chemical Physics

journal homepage: www.elsevier.com/locate/chemphys

A combined INS and DINS study of proton quantum dynamics of ice and water across the triple point and in the supercritical phase

C. Andreani [a], G. Romanelli [a,*], R. Senesi [a,b]

[a] Università degli Studi di Roma "Tor Vergata", Dipartimento di Fisica and Centro NAST, via della Ricerca Scientifica 1, 00133 Roma, Italy
[b] CNR–IPCF Sez. di Messina, Italy

ARTICLE INFO

Article history:
Available online 13 August 2013

Keywords:
Hydrogen bond
Proton potential
Inelastic Neutron Scattering

ABSTRACT

We report new results of a combined analysis of previous Inelastic Neutron Scattering (INS) and Deep Inelastic Neutron Scattering (DINS) experiments on ice at $T = 271$ K and water at $T = 285$ K and $T = 673$ K. Proton quantum dynamics is discussed in terms of the total mean kinetic energy, $\langle E_K \rangle$, and its three principal direction components, $\langle E_K \rangle_\alpha$ (with $\alpha = x, y, z$), the lineshape momentum distribution, $n(p)$, and its harmonic lineshape components, $n_h(p)$. The results show that the single proton dynamics is ground-state dominated and that $\langle E_K \rangle_x$, $\langle E_K \rangle_y$ and $\langle E_K \rangle_z$ consist mainly of weighted averages of a mix of bending and librational, librational and stretching mean kinetic energy components, respectively. The stretching component $\langle E_K \rangle_z$ is redshifted respect to its harmonic component due to additional network mode contributions and softening caused by anharmonicity. The $n(p)$ lineshapes derived at the investigated temperature reflect the anisotropy and quasi-harmonic nature of proton motion in ice and water.

1. Introduction

Detailed description of the structure and dynamics of the hydrogen-bond network in water is essential to reach a thorough understanding of the unique properties of this liquid, necessary both for the evolution of life and its continuance. The water properties are brought about by the hydrogen bonded environment, in a picture where each molecule is involved in about four hydrogen bonds with strengths considerably less than covalent bonds but considerably greater than the natural thermal energy. Hydrogen bonds are roughly tetrahedrally arranged with the possibility that, when strongly formed, the local clustering expands and density decreases. Evidence of the particular uniqueness of liquid water are in its many physical and chemical properties which occur for instance when low density structuring naturally occurs at low and supercooled temperatures.

The dynamics of the proton that participates in hydrogen bonding is a subject of great interest and the quantum effects associated with protons have a significant impact on the behavior of hydrogen bond networks. Quantum effects influence the vibrational dynamics probed in Inelastic Neutron Scattering, i.e. the protons participating in H-bonds, as well as the static properties of ice and water, with the quantal behavior originating from zero-point motion. It has been recently suggested that a detailed description of the strength of the hydrogen bond is a prerequisite to elucidate the influence of quantum nuclear effects on the hydrogen bonding [1]. The picture proposed is that this effect arises from a competition between anharmonic quantum fluctuations of intermolecular bond bending and intramolecular covalent bond stretching, where the latter fluctuations tend to strengthen H-bonds whereas the former to weaken H-bonds. Quantum effects, such as those associated with the breaking and distortion of hydrogen bonds are uniquely revealed by using Deep Inelastic Neutron Scattering (DINS), also called Neutron Compton Scattering (NCS) [3–5], measuring the proton momentum distributions, $n(p)$, and mean kinetic energy, $\langle E_K \rangle$. In parallel novel simulation techniques have been also employed to calculate the $n(p)$, using state of the art open path integral simulations [6,7] implemented with first principles molecular dynamics [8] within the Path Integral Car–Parrinello Molecular Dynamics (PICPMD) framework [9]. These theoretical calculations have been able to successfully reproduce the hydrogen momentum distribution in ice Ih [10]. However none of the existing electrostatic models, treating the intermolecular potential as unchanged by hydrogen bonding, are accurate enough to fully reproduce the experimentally determined $n(p)$ and $\langle E_K \rangle$ of Ref. [11,12] as well as DINS results from metastable water as those shown in Ref. [13,14], and they are still awaiting a proper theoretical description. Over all in recent years several are the DINS and PICPMD investigations devoted to study both physical quantities in ice and water in a wide temperature range 269 K $< T <$ 673 K [3,7,10,13–22]. In the experimental studies one makes use of

* Corresponding author. Tel.: +39 06 7259 4429.
E-mail address: giovanni.romanelli@uniroma2.it (G. Romanelli).

0301-0104/$ - see front matter © 2013 Elsevier B.V. All rights reserved.
http://dx.doi.org/10.1016/j.chemphys.2013.07.009

incident neutrons in the range 1–100 eV, and scattered wavevectors in the range of 20 Å^{-1} < q < 250 Å^{-1} to measure the $n(p)$ lineshape of light and heavy ions [23,24]. The $n(p)$, the diffraction pattern of the proton wave function, in nearly all cases is determined by the ground vibrational state of the protons. Hence it provides a unique probe of the effective potential the proton experiences in its local environment [3].

Inelastic Neutron Scattering (INS), currently used to determine the vibrational spectra of hydrogen bonded systems, is a technique which provides rather comprehensive, quantitative and more direct information on the vibrational spectrum through the measurement of the dynamical structure factor. The latter quantity is directly related to the density of vibrational states, weighted by the squared amplitudes of the atomic oscillations [25–27]. Hence using INS one can measure not only translational, librational and intra-molecular excitations energies but also spectral intensities. In this paper we will show that INS experiments at high incident energies and low momentum transfer can be also used to obtain additional and complementary information to DINS on the quantum nature of $n(p)$ and $\langle E_K \rangle$.

Values of proton mean kinetic energy and momentum distributions can also be calculated using empirical models. In the latter case the frequencies of a set of decoupled quantum harmonic oscillators are derived from optical data and hydrogen projected vibrational neutron spectra, under the assumptions of decoupling between translational, rotational and vibrational degrees of freedom. This procedure has been already employed in solid and liquid H_2S [28] and in supercritical water [29]. In the harmonic calculations the average number of excited phonons, at the given temperature, determines the contribution of each harmonic oscillator to the $\langle E_K \rangle$.

This paper reports a study of the proton single particle dynamics in ice at T = 271 K and water at T = 285 K and T = 673 K performed by a combined and additional analysis of DINS and INS data from Refs [14,10,2]. Section 2 describes the experiments and data analysis, Section 3 presents and discusses results of the study and conclusions.

2. INS and DINS experiments and data analysis

Recent DINS and INS experiments on ice and liquid water have been performed on the VESUVIO spectrometer at the ISIS spallation neutron source (UK) [4] on an attosecond time scale (i.e. 10^{-15} s–10^{-16} s) – at T = 271 K [10], T = 285 K [14] and T = 673 K [22] – and on the time-of-flight neutron Chopper spectrometer SEQUOIA at the Spallation Neutron Source (SNS) – at T = 271 K and T = 285 K [2] – using an incident neutron energy of the chopper of E_i= 600 meV, respectively. Full details of the experimental set up of both measurements can be found in Ref. [14,10,22,2].

The $n(p)$ lineshapes for this set of DINS data have been fitted using the spherical average of an anisotropic Gaussian distribution [10]:

$$n(p) = \left\langle \frac{1}{\sqrt{8\pi^3}\sigma_x\sigma_y\sigma_z} \exp\left(-\frac{p_x^2}{2\sigma_x^2} - \frac{p_y^2}{2\sigma_y^2} - \frac{p_z^2}{2\sigma_z^2} \right) \right\rangle_\Omega \quad (1)$$

with $\langle A \rangle_\Omega$ being the solid angular average of A.

Using this equation for each temperature three variances σ_α^2 (with $\alpha = x, y, z$) have been obtained fitting the $n(p)$ line shapes of DINS data from Ref. [14,10,22]. These variances can then be related to three components of the mean kinetic energy, $\langle E_K \rangle_\alpha$, or to the three effective principal frequencies, ω_α, through the following expression [10]:

$$\frac{\hbar^2\sigma_\alpha^2}{2M} = \langle E_K \rangle_\alpha = \frac{\hbar\omega_\alpha}{4} \coth\left(\frac{\hbar\omega_\alpha}{2K_BT} \right) \quad (2)$$

Table 1 reports values of $\langle E_K \rangle_\alpha$, total mean kinetic energy $\langle E_K \rangle$ and ω_α for ice and water derived from Eq. (1) and Eq. (2). For T = 673 K we also report the total mean kinetic energy values obtained in Refs. [15,22], by expressing the $n(p)$ in terms of the generalized Laguerre polynomials. At T = 673 K values of ω_α from Ref. [17] are also listed. These effective frequencies agree, within the statistical accuracy, with those obtained in this work. We stress that the algorithm developed in the present analysis makes use of a finer angular mesh than that used in Ref. [17], which reduces the uncertainties due to the correlation matrix and thus the uncertainties of the individual ω_α.

As far as the INS data are concerned, the corrected one-phonon incoherent dynamical structure factor, $S_{inc}(\theta,\omega)$ from Ref. [2] are reported in Fig. 1 for ice, at T = 271 K, and for water, at T = 285 K. These functions can be expressed in terms of the energy and wavevector transfers, $E = \hbar\omega$ and $q = k_i - k_f$, with k_f and k_i being the final and incident neutron wavevectors, to yield the $S_{inc}(q,E)$ functions. By performing extrapolations of $S_{inc}(q,E)$ functions at fixed E values for $q \to 0$ one obtains, within the harmonic approximation, the hydrogen projected density of states g_{exp}(E) using the relation [25]:

$$g_{exp}(E) = lim_{q\to 0} \frac{S_{inc}(q,E)}{q^2} 2ME \frac{e^{[2W(q)]}}{[n(E)+1]} \quad (3)$$

with M being the proton mass, $n(E)$ the Bose population factor. Full details of this procedure are described in previous papers [25,2]. From the OH stretching components of the hydrogen projected density of states, $g_{exp}(E)_{OH}$, as calculated in Ref. [2], one can derive the proton mean kinetic energy for the OH stretching:

$$\langle E_K \rangle_{OH} = \frac{3}{4} \int_{355}^{480} g_{exp}(E)_{OH} E dE = \frac{3\hbar^2}{2M} \sigma_{OH}^2 \quad (4)$$

$\langle E_K \rangle_{OH}$ values for ice at T = 271 K and water at T = 285 K from Eq. (4) are reported in Table 2. For liquid water at T = 673 K the $\langle E_K \rangle_{OH}$ value has been derived using the $g_{exp}(E)_{OH}$ lineshape from Fig. 4 of INS data of Ref [30]. The value, $\langle E_K \rangle_{OH}$=115 ± 5, is also reported in Table 2.

From INS vibrational spectra an independent set of effective principal frequencies ω_α can also be calculated as follows. Within

Table 1
Ice, T = 271 K: ω_α from Ref. [10]; the total kinetic energy $\langle E_K \rangle$ and corresponding three components of the mean kinetic energies, $\langle E_K \rangle_\alpha$ are calculated from Eq. (2). Water at T = 285 K: DINS data from Ref. [14] with $\langle E_K \rangle_\alpha$ calculated fitting the $n(p)$ lineshape according to Eq. (1); corresponding three effective frequencies, ω_α, calculated from Eq. (2) and total kinetic energy $\langle E_K \rangle$. Water, T = 673 K: DINS data from Ref. [22] with $\langle E_K \rangle_\alpha$ calculated fitting the $n(p)$ lineshape according to Eq. (1); corresponding three effective frequencies, ω_α, calculated from Eq. (2) and total kinetic energy $\langle E_K \rangle$; values of $\langle E_K \rangle$ from DINS data of Ref. [15] and Ref. [22] are also listed. Values $of\omega_\alpha$ from Ref. [17] are also listed.

T [K]			ω_x [meV]	ω_y [meV]	ω_z [meV]	$\langle E_K \rangle_x$ [meV]	$\langle E_K \rangle_y$ [meV]	$\langle E_K \rangle_z$ [meV]	$\langle E_K \rangle$ [meV]
Ice	271	DINS [10]	114 ± 10	152 ± 13	347 ± 11	28.9 ± 2.1	38.1 ± 3.1	86.7 ± 2.7	153.7 ± 2
Water	285	DINS [14]	63 ± 9	207 ± 17	335 ± 10	18.3 ± 1.8	51.8 ± 4.0	83.8 ± 2.5	153.9 ± 3
	673	DINS	69 ± 13	193 ± 20	368 ± 17	32.3 ± 3.6	51.8 ± 5.0	92.5 ± 4.2	176.6 ± 4
		DINS [17,22]	120 ± 29	255 ± 97	330 ± 83				1780 ± 4
		DINS [15]							178.0 ± 11

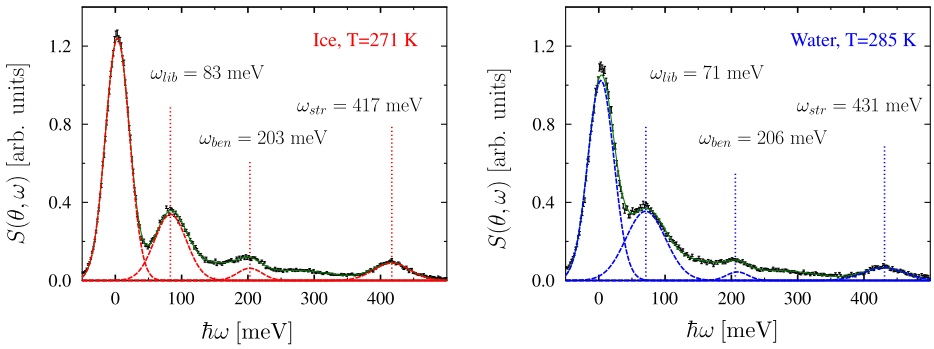

Fig. 1. The $S_{inc}(\theta,\omega)$ dynamical structure factors from INS experiments of Ref. [2] are plotted as black dots for ice at $T = 271$ K (left panel) and water at $T = 285$ K (right panel) together with the Multi-Gaussian fits (green lines). The individual line shapes corresponding to elastic, libration, bending and stretching modes for ice and water are also plotted as red dashed line in the left panel and as blue dashed line in the right panel, respectively. Values for ω_{lib}, ω_{ben} and ω_{str} for ice and water resulting from the Multi-Gaussian fits of both spectra are also reported. (For interpretation of the references to colour in this figure legend, the reader is referred to the web version of this article.)

Table 2
Values of ω_α from Eq. 5 and INS data of Ref. [2], obtained fitting spectra of Fig. 1 of ice at $T = 271$ K (left panel) and water at $T = 285$ K (right panel) and corresponding component $\langle E_K\rangle_z$ obtained using Eq. 2; the stretching kinetic energy component $\langle E_K\rangle_{OH}$ is obtained from Eq. (4). Values for ω_α from Raman data of Ref. [30] for water at $T = 673$ K and the stretching kinetic energy component $\langle E_K\rangle_{OH}$ is obtained from Ref. [30] (see text).

T [K]			ω_x [meV]	ω_y [meV]	ω_z [meV]	$\langle E_K\rangle_z$ [meV]	$\langle E_K\rangle_{OH}$ [meV]
Ice	271	INS	83 ± 2	143 ± 5	417 ± 5	104 ± 1.2	98 ± 4
Water	285	INS	72 ± 3	139 ± 8	429 ± 6	107 ± 1.5	100 ± 4
	673	Raman	59	130	445	113	115 ± 5

the assumption of decoupled quantum translational, rotational and vibrational harmonic oscillators [15], $S_{inc}(\theta,\omega)$ data set are fitted to derive three principal vibrational frequencies, i.e. $\omega_{lib}, \omega_{ben}$ and ω_{str}. Let us apply this procedure for the INS data set of Ref. [2]. Multi-Gaussian fits of the $S_{inc}(\theta,\omega)$ spectra for ice, at $T = 271$ K, and water, at $T = 285$ K are plotted in Fig. 1 as a green line. In the same figure the individual line shapes for the principal vibrational frequencies are also reported for ice, as red dashed line, and for water, as blue dashed line. The distinct features of the Multi-Gaussian fit of ice INS spectrum as compared to Multi-Gaussian fit of water INS spectrum are highlighted in Fig. 2. In this figure one can appreciate a redshift of the stretching and bending bands, i.e. $\Delta\hbar\omega_{str} = 12$ meV and $\Delta\hbar\omega_{ben} = 3$ meV, and a blueshift of the vibrational bands, i.e. $\Delta\hbar\omega_{lib} = 12$ meV. We now make use of the values of the principal vibrational frequencies resulting from the fit to INS spectra to calculate an independent set of three effective principal frequencies, ω_α, as follows:

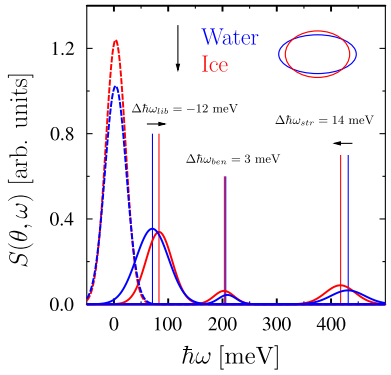

Fig. 2. Multi-Gaussian fits of the $S_{inc}(\theta,\omega)$ spectra from INS experiment of Ref. [2] for ice at $T = 271$ K (red line) and water at $T = 285$ K (blue line), for a scattering angle $\theta = 20°$. (For interpretation of the references to colour in this figure legend, the reader is referred to the web version of this article.)

$$\begin{aligned}\omega_x &= \omega_{lib}\\ \omega_y &= \frac{1}{2}(\omega_{lib}+\omega_{ben})\\ \omega_z &= \omega_{str}\end{aligned} \tag{5}$$

These expressions are exact in the limit of infinite mass for the oxygen atom, and in the limit of $\hbar\omega_i \gg 2K_BT$, where $i = lib, ben$ and str.

For ice at $T = 271$ K and water at $T = 285$ K values of ω_α and $\langle E_K\rangle_z$, derived from ω_z using Eq. (2), are reported in Table 2. For water at $T = 673$ K the values of ω_α listed in the table are from Raman spectroscopic data of Ref. [30]. For the librational mode, a simple average of the three librational Raman frequencies has been considered.

We now recall that nine is total number of degrees of freedom of one water molecule and that the classical translational contribution is $\frac{3}{2}K_BT$, with a fraction $\frac{1}{18}$ being associated to the hydrogen atom. Labeling ω_{lib} the rotational contribution and ω_{str} the average contribution due to the symmetric and anti-symetric stretching modes, the directional contributions to the total kinetic energy can be written as follows [28]:

$$\begin{aligned}\langle E_K\rangle_x &= 2S_{lib}\frac{\hbar\omega_{lib}}{4}\coth\left(\frac{\hbar\omega_{lib}}{2K_BT}\right)+S_{tra}\frac{1}{2}K_BT\\ \langle E_K\rangle_y &= S_{lib}\frac{\hbar\omega_{lib}}{4}\coth\left(\frac{\hbar\omega_{lib}}{2K_BT}\right)+S_{ben}\frac{\hbar\omega_{ben}}{4}\coth\left(\frac{\hbar\omega_{ben}}{2K_BT}\right)+S_{tra}\frac{1}{2}K_BT\\ \langle E_K\rangle_z &= 2S_{str}\frac{\hbar\omega_{str}}{4}\coth\left(\frac{\hbar\omega_{str}}{2K_BT}\right)+S_{tra}\frac{1}{2}K_BT\end{aligned} \tag{6}$$

with S_α being the fractions of kinetic energy as defined by an harmonic model for the free molecule [29]. The calculated values for $\langle E_K\rangle_\alpha$ according to Eq. (6) and the total mean kinet energy $\langle E_K\rangle$ are reported in Table 3,, together with the corresponding values for the DINS data from Table 1 and the $\langle E_K\rangle_{OH}$ from Table 2. In the last column of Table 3 we calculate the ratio between the OH stretching mean kinetic energy, from INS analysis, and the total mean kinetic

Table 3
Values of $\langle E_K\rangle_\alpha$ and total kinetic energy $\langle E_K\rangle$ from DINS data of Ref. [10] for ice at $T = 271$ K and water at $T = 285$ K and $T = 673$ K. The three INS components of the mean kinetic energies, $\langle E_K\rangle_\alpha$, and the total kinetic energy $\langle E_K\rangle$ for ice at $T = 271$ K and water at $T = 285$ K have been obtained using values from the fit of Fig. 1 and Eq. 6. The same values but for water at $T = 673$ K have been obtained applying Eq. 6 to Raman values of [30]. The stretching kinetic energy component $\langle E_K\rangle_{OH}$ is as in Table 1. In the last column, the ratio $\frac{\langle E_K\rangle_{OH}}{\langle E_K\rangle_{DINS}}$ (blue color), between the OH stretching mean kinetic energy from INS analysis and total mean kinetic energy from DINS analysis, is also reported.

T [K]			$\langle E_K\rangle_{OH}$ [meV]	$\langle E_K\rangle_x$ [meV]	$\langle E_K\rangle_y$ [meV]	$\langle E_K\rangle_z$ [meV]	$\langle E_K\rangle$ [meV]	$\frac{\langle E_K\rangle_{OH}}{\langle E_K\rangle_{DINS}}$
Ice	271	INS	98 ± 4	21.6 ± 0.3	34.4 ± 1.2	98.8 ± 1.2	154.8 ± 1.0	
		DINS		28.9 ± 2.1	38.1 ± 3.1	86.7 ± 2.7	153.7 ± 2.0	0.64
Water	285	INS	100 ± 4	19.4 ± 0.3	33.5 ± 1.9	101.7 ± 1.5	154.6 ± 1.4	
		DINS		18.3 ± 1.8	51.8 ± 4.0	83.8 ± 2.5	153.9 ± 3	0.65
	673	Raman	115 ± 5	31.4	39.4	107.9	178.7	
		DINS		32.3 ± 3.6	51.8 ± 5.0	92.5 ± 4.2	176.6 ± 4	0.65
		DINS [22]					178.0 ± 4	
		DINS [15]					178.0 ± 11	

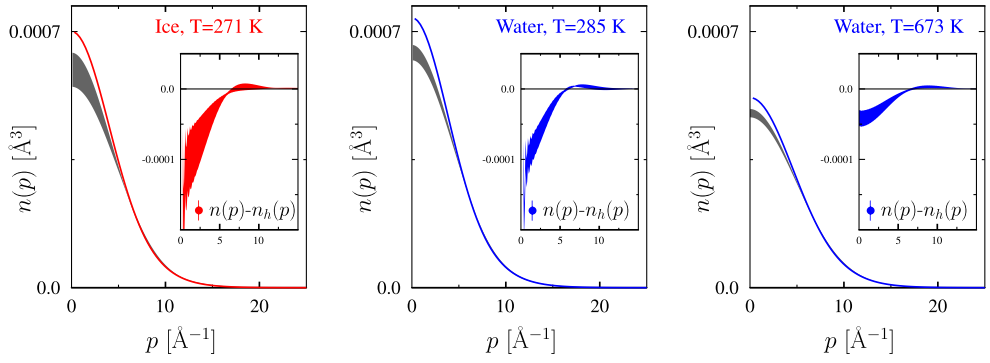

Fig. 3. Plot of the $n(p)$ line shapes for ice and water (black lines) for DINS data (from Eq. (1), see text) and their harmonic components, $n_h(p)$, from INS and Raman data (see text): ice (left panel, red line), water (central and right panels, blue lines). The difference $[n(p)\text{-}n_h(p)]$ is also plotted in the inserts at each temperature. (For interpretation of the references to color in this figure legend, the reader is referred to the web version of this article.)

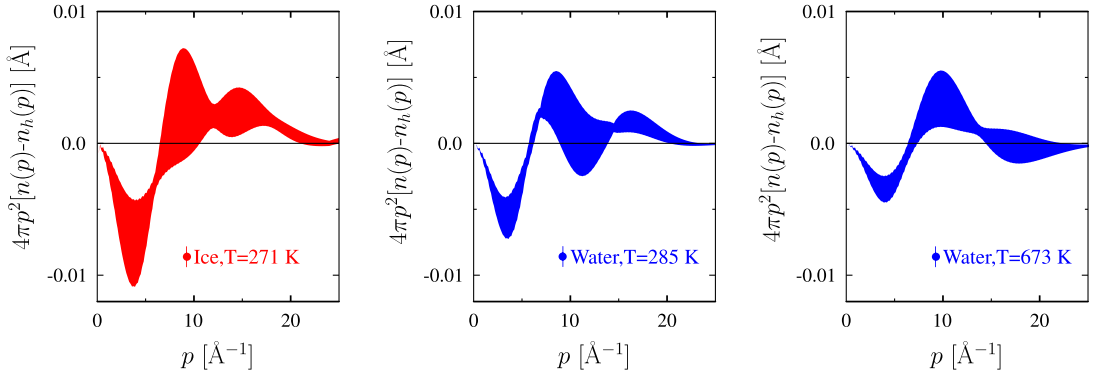

Fig. 4. Plots of the difference $4\pi p^2[n(p) - n_h(p)]$ for ice (left panel) and water (central and right panel).

energy, from DINS analysis, $\frac{\langle E_K\rangle_{OH}}{\langle E_K\rangle_{DINS}}$, for ice and water at the investigated temperatures. From this Table at all temperatures we can appreciate a quite good agreement between $\langle E_K\rangle_z$ values obtained from Eq. (6) and $\langle E_K\rangle_{OH}$ values of derived independently from the OH stretching components of the hydrogen projected density of states through Eq. (4).

From the $\langle E_K\rangle_\alpha$ DINS, INS and Raman values of Table 1 and Table 2 one can retrieve the variances σ^2_α, via Eq. (2), and further can derive the proton momentum distribution, $n(p)$ and the harmonic components of proton momentum distribution $n_h(p)$. The radial component of both momentum distribution line shapes, i.e $4\pi p^2 n(p)$ and $4\pi p^2 n_h(p)$, are plotted for ice at $T = 271$ K in the left panel of Fig. 3 in black and red color,For interpretation of color in Fig. 3, the reader is referred to the web version of this article. respectively, and for water at $T = 285$ K and $T = 673$ K in the central and right panels of the same figure in back and blue color, respectively.

3. Results and conclusions

A first comment is relative to the values of the total mean kinetic energy of ice and water, $\langle E_K\rangle$, reported in the penultimate column of Table 3, which have been derived from the analysis of independent INS and DINS data sets through Eqs. (2) and (6). These

values result in a satisfactory agreement for all the investigated temperatures, within the statistical accuracy.

The stretching components of the mean kinetic energy derived from INS data for ice at $T = 271$ K and water at $T = 285$ K through Eq. (6), $\langle E_K \rangle_z$, are in excellent agreement with $\langle E_K \rangle_{OH}$ at the same temperatures derived in Ref. [2] from the OH stretching components of the hydrogen projected density of states, $g_{exp}(E)_{OH}$, through Eq. (3). This confirms the reliability of the harmonic description of Eq. (6) used to calculate the individual components $\langle E_K \rangle_\alpha$ in the present study and to describe the mean kinetic energy components in a previous study of H_2S [28]. In Table 3 we observe that the stretching components $\langle E_K \rangle_z$ are redshifted in respect to their relative harmonic components at all investigated temperatures. This finding, already emerged in a recent DINS study of ice at $T = 271$ K [10], is interpreted as due to additional network mode contributions and softening caused by anharmonicity. Further in Table 3 the $\langle E_K \rangle_y$ DINS components show a clear blue shift, larger in water than in ice, with respect to the corresponding $\langle E_K \rangle_y$ INS components. This finding supports a picture with weaker hydrogen bond network in liquid phase than in ice.

The $n(p)$ lineshape, as derived from DINS, and its harmonic component, $n_h(p)$, derived from the INS analysis, are shown in Fig. 3 for ice at $T = 271$ K and water at $T = 285$ K and $T = 673$ K with their experimental error. For each temperature, the harmonic components have been plotted as a red line for ice (left panel) and as a blue line for water (central and right panels). The difference between the two line shapes $[n(p) - n_h(p)]$ are also plotted. The two lineshapes differ significantly for $p \leqslant 5$ Å^{-1}, minor differences are found in the range 6 Å^{-1} to 10 Å^{-1} and beyond 10 Å^{-1}. These differences are better emphasized in the radial representation of the $n(p)$ lineshape, $4\pi p^2[n(p) - n_h(p)]$, plotted in Fig. 4. One comment regards the anisotropy of the $n(p)$ functions, as fingerprinted in the different values of the three variances σ_α^2, i.e. of the three $\langle E_K \rangle_\alpha$ in Table 3 derived from Eq. (2). In Fig. 2 this feature is clearly highlighted by both the decrease of the stretching frequency value and the increase of librational frequency value and by the shape of the two ellipsoids, red for ice and blue for water, schematically plotted at the top right corner of the figure. In conclusion $n(p)$ lineshapes derived at the investigated temperature reflect the anisotropy and quasi-harmonic nature of proton motion in ice and water.

The last column of Table 3 shows the ratio $\frac{\langle E_K \rangle_{OH}}{\langle E_K \rangle_{DINS}}$, where the $\langle E_K \rangle_{DINS}$ is that obtained in the present study, i.e. by the sum of the three $\langle E_K \rangle_\alpha$ components fitted to the $n(p)$ line shapes through Eq. (1). The latter procedure highlights the contributions from intramolecular modes, in particular of the OH stretching, to the hydrogen motion in a way more directly related to a deckled harmonic model than using $\langle E_K \rangle$ values obtained by Gauss–Hermite fits as in Ref. [15,22].

This study although confirms the effectiveness of the DINS techniques to provide quantitative values of $n(p)$ and $\langle E_K \rangle$ further shows how a combined use of DINS and INS can provide additional and unique information on the harmonic components of these physical quantities.

Acknowledgments

This work was partially supported within the CNR-STFC Agreement No. 06/20018 concerning collaboration in scientific research at the spallation neutron source ISIS (Rutherford Appleton Laboratory, UK) and with the support of META (Materials Enhancement for Technological Applications) PIRSES-GA-2010-269182, Marie Curie Actions, People, VII Framework Programme.

References

[1] X.-Z. Li, B. Walker, A. Michaelides, Quantum nature of the hydrogen bond, Proc. Nat. Acad. Sci. 108 (2011) 6369–6373.
[2] R. Senesi, D. Flammini, A.I. Kolesnikov, E.D. Murray, G. Galli, C. Andreani, The quantum nature of the oh stretching mode in ice and water probed by neutron scattering experiments, J. Chem. Phys. (2013). accepted for publication.
[3] C. Andreani, D. Colognesi, J. Mayers, G.F. Reiter, R. Senesi, Adv. Phys. 54 (2005) 377.
[4] R. Senesi, C. Andreani, Z. Bowden, D. Colognesi, E. Degiorgi, A.L. Fielding, J. Mayers, M. Nardone, J. Norris, M. Praitano, N.J. Rhodes, W.G. Stirling, J. Tomkinson, C. Uden, Phys. B Condens. Matter 276 (2000) 200.
[5] J. Mayers, G. Reiter, Meas. Sci. Technol. 23 (2012) 045902.
[6] J.A. Morrone, R. Car, Phys. Rev. Lett. 101 (2008) 017801.
[7] J.A. Morrone, L. Lin, R. Car, J. Chem. Phys. 130 (2009) 204511.
[8] R. Car, M. Parrinello, Phys. Rev. Lett. 55 (1985) 2471.
[9] D. Marx, M. Parrinello, Z. Phys. B Condens. Matter 95 (1994) 143.
[10] D. Flammini, A. Pietropaolo, R. Senesi, C. Andreani, F. McBride, A. Hodgson, M.A. Adams, L. Lin, R. Car, J. Chem. Phys. 136 (2012) 024504.
[11] C.J. Burnham, G.F. Reiter, J. Mayers, T. Abdul-Redah, H. Reichert, H. Dosch, Phys. Chem. Chem. Phys. (Incorporating Faraday Transactions) 8 (2006) 3966.
[12] C.J. Burnham, T. Hayashi, R.L. Napoleon, T. Keyes, S. Mukamel, G.F. Reiter, The proton momentum distribution in strongly H-bonded phases of water: a critical test of electrostatic models, J. Chem. Phys. 135 (2011).
[13] A. Pietropaolo, R. Senesi, C. Andreani, A. Botti, M.A. Ricci, F. Bruni, Phys. Rev. Lett. 100 (2008) 127802.
[14] A. Pietropaolo, R. Senesi, C. Andreani, J. Mayers, Braz. J. Phys. 39 (2009) 318.
[15] C. Andreani, D. Colognesi, E. Degiorgi, M.A. Ricci, J. Chem. Phys. 115 (2001) 11243.
[16] A. Pietropaolo, R. Senesi, C. Andreani, A. Botti, M.A. Ricci, F. Bruni, Phys. Rev. Lett. 103 (2009) 069802.
[17] C. Andreani, D. Colognesi, A. Pietropaolo, R. Senesi, Chem. Phys. Lett. 518 (2011) 1.
[18] D. Colognesi, C. Andreani, E. Degiorgi, J. Neutron Res. 11 (2003) 123.
[19] M. Ceriotti, G. Bussi, M. Parrinello, Phys. Rev. Lett. 103 (2009) 030603.
[20] L. Lin, J.A. Morrone, R. Car, M. Parrinello, Phys. Rev. Lett. 105 (2010) 110602.
[21] L. Lin, J.A. Morrone, R. Car, M. Parrinello, Phys. Rev. B 83 (2011) 220302.
[22] C. Pantalei, A. Pietropaolo, R. Senesi, S. Imberti, C. Andreani, J. Mayers, C. Burnham, G. Reiter, Phys. Rev. Lett. 100 (2008) 177801.
[23] M. Ceriotti, D.E. Manolopoulos, Phys. Rev. Lett. 109 (2012) 100604.
[24] M. Ceriotti, G. Miceli, A. Pietropaolo, D. Colognesi, A. Nale, M. Catti, M. Bernasconi, M. Parrinello, Phys. Rev. B 82 (2010) 174306.
[25] C. Andreani, P. Bosi, F. Sacchetti, C.K. Loong, J. Chem. Phys. 83 (1985) 750.
[26] C. Andreani, V. Merlo, M.A. Ricci, Nucl. Instrum. Methods Phys. Res. B 36 (1989) 216.
[27] C. Andreani, V. Merlo, M.A. Ricci, B.C. Boland, Mol. Phys. 66 (1989) 747.
[28] C. Andreani, E. Degiorgi, R. Senesi, F. Cilloco, D. Colognesi, J. Mayers, M. Nardone, E. Pace, J. Chem. Phys. 114 (2001) 387.
[29] R. Moreh, D. Nemirovsky, J. Chem. Phys. 133 (2010) 084506.
[30] M.A. Ricci, M. Nardone, A. Fontana, C. Andreani, W. Hahn, Light and neutron scattering studies of the OH stretching band in liquid and supercritical water, J. Chem. Phys. 108 (1998) 450.